Biosensors and Bioelectronics 43 (2013) 69–74

Contents lists available at SciVerse ScienceDirect

Biosensors and Bioelectronics

journal homepage: www.elsevier.com/locate/bios

Detection of lead (II) with a "turn-on" fluorescent biosensor based on energy transfer from CdSe/ZnS quantum dots to graphene oxide

Ming Li [a], Xuejiao Zhou [b], Shouwu Guo [b], Nianqiang Wu [a,*]

[a] Department of Mechanical and Aerospace Engineering, West Virginia University, Morgantown, WV 26506-6106, USA
[b] National Key Laboratory of Micro/Nano Fabrication Technology, Key Laboratory for Thin Film and Microfabrication of the Ministry of Education, Research Institute of Micro/Nano Science and Technology, Shanghai Jiao Tong University, Shanghai 200240, PR China

ARTICLE INFO

Article history:
Received 25 September 2012
Received in revised form
20 November 2012
Accepted 30 November 2012
Available online 7 December 2012

Keywords:
Sensor
Fluorescence
Energy transfer
Graphene oxide
Quantum dot
Lead

ABSTRACT

Graphene oxide (GO) sheets are mixed with the aptamer-functionalized CdSe/ZnS quantum dots (QDs). Consequently, the aptamer-conjugated QDs bind to the GO sheets to form a GO/aptamer-QD ensemble, which enables the energy transfer from the QDs to the GO sheets, quenching the fluorescence of QDs. The GO/aptamer–QD ensemble assay acts as a "turn-on" fluorescent sensor for Pb^{2+} detection. When Pb^{2+} ions are present in the assay, the interaction of Pb^{2+} with the aptamer induces a conformational change in the aptamer, leading to the formation of a G-quadruplex/Pb^{2+} complex. As a result, the QDs that are linked to the G-quadruplex/Pb^{2+} complex are detached from the GO sheet, which "turns on" the fluorescence of the QDs. This sensor exhibits a limit of detection of 90 pM and excellent selectivity toward Pb^{2+} over a wide range of metal ions. The experiments have provided direct evidence that the fluorescence of QDs is quenched by GO *via* the nano-metal surface energy transfer (NSET) mechanism rather than the conventional Förster resonance energy transfer (FRET) process.

1. Introduction

In traditional sensors based on fluorescence resonance energy transfer (FRET), organic dye molecules are usually used as both the energy donor and the acceptor (Crivat et al., 2010; Li et al., 2011e; Liu and Lu, 2002). However, organic dyes are vulnerable to photobleaching. Inorganic quantum dots (QDs) therefore have received intensive attention as an optional energy donor (Li et al., 2011c; Gaponik et al., 2010; Medintz et al., 2006) because QDs exhibit good resistance to photobleaching, narrow emission band, broad absorption spectra and size-tunable emission as compared to organic dyes (Tan et al., 2003; Wang et al., 2010a; Zhao et al., 2011a). It is well-known that traditional FRET sensors have a limited detectable distance of ~6 nm (Yun et al., 2005). Therefore gold nanoparticles have been explored as an alternative energy acceptor to substitute for organic dyes (Darbha et al., 2007; Dulkeith et al., 2005; Jennings et al., 2006; Li et al., 2011c, 2011d; Quach et al., 2011). It has been demonstrated that gold nanoparticles can quench the fluorescence emission of the energy donor in a much longer quenching distance (Li et al., 2011d), which enables the energy transfer-based fluorescent sensor to act as a spectroscopic ruler for probing the distance-dependent properties of macromolecules (Ling and Huang, 2010). Recently graphene and graphene oxide (GO) emerged as the new energy acceptors for energy transfer-based fluorescent sensors (Dong et al., 2010; Loh et al., 2010; Zhang et al., 2011a). Theoretical calculations have shown that the energy transfer from a fluorescent dye to graphene follows the nano-metal surface energy transfer (NSET) mechanism, which is similar to the energy transfer to a gold nanoparticle (Swathi and Sebastian, 2008, 2009). GO shows super quenching capability as an energy acceptor. The efficient quenching distance is estimated to reach up to 30 nm, which provides great flexibility for construction of fluorescent sensors on the nanoscale. Owing to these unique features, several GO-based biosensors have been developed for detection of biomolecules, cation ions and small molecules (Chen et al., 2011; De et al., 2011; Kong et al., 2011; Li et al., 2012a; Lu et al., 2009; Shi et al., 2011; Wang et al., 2010b). GO is an amazing optical sensing material that can serve either as an energy acceptor (in this work) or as an energy donor (Li et al., 2013) or a fluorophore (Li et al., 2012d).

In the present work, a "turn-on" fluorescent sensor based on the QD/aptamer–GO ensemble is constructed in order to detect the Pb^{2+} ions. In this sensor, an aptamer, which specifically binds to Pb^{2+} (Li et al., 2010a, 2010b, 2011a; Jiang et al., 2010), is employed as the molecular recognition probe. The CdSe/ZnS QD acts as the energy donor. GO serves as the energy acceptor since GO has excellent water-solubility, flexible surface-modification capability and low-cost of manufacturing (Balapanuru et al., 2010; Lee et al., 2011; Li et al., 2011b; Stankovich et al., 2006;

* Corresponding author. Fax: +1 304 293 6689.
E-mail address: nick.wu@mail.wvu.edu (N. Wu).

0956-5663/$ - see front matter © 2012 Elsevier B.V. All rights reserved.
http://dx.doi.org/10.1016/j.bios.2012.11.039

Wang et al., 2011; Xiang et al., 2013). In addition, the large two-dimensional (2-D) aromatic surface of GO is an appealing substrate for conjugation of certain biomolecules (Peng et al., 2010; Wei et al., 2012; Zhang et al., 2011b, 2011c). Even without any further surface modification, GO can conjugate with single-stranded DNA (ssDNA) *via* the π–π stacking interactions between the aromatic nucleobases of ssDNA and the sp^2-bonded carbon atoms of GO (Guo and Dong, 2011; Patil et al., 2009; Wang et al., 2011). Therefore, GO is an attractive substrate for immobilization of the aptamer conjugated with the QDs. Pb^{2+} is selected as the target analyte since it is one of the most toxic environmental pollutants. Exposure of human to Pb^{2+} can cause serious damage to the brain, kidneys, nervous system and red blood cells (Goyer, 1993). Children are more prone to the poisoning of lead. Lead interferes with the development of the central nervous system (CNS), leading to potentially permanent learning and behavior disorders (Goyer, 1993). Hence, it is essential to develop a highly sensitive and cost-effective sensor for rapid detection of Pb^{2+}.

2. Materials and methods

2.1. Chemicals

All DNAs and the aptamer with the sequence of 5′–NH_2–$(CH_2)_6$–GGGTGGGTGGGTGGGT–3′, which was reported to specifically bind to Pb^{2+} (Li et al., 2010a, 2011a), were ordered from Integrated DNA Technologies (IDT, Coralville, IA). *N*-hydroxysuccinimide (NHS), 1-ethyl-3-(3-dimethylaminopropyl)-carbodiimide (EDC), $Cu(NO_3)_2$, $Hg(NO_3)_2$, $Pb(NO_3)_2$, $Cd(NO_3)_2 \cdot 4H_2O$, $Co(NO_3)_2 \cdot 6H_2O$ and 5 M NaCl stock solution were purchased from Sigma-Aldrich (St. Louis, MO). KI (99.9%), $AgNO_3$ (Premion, 99.995%), $Fe(NO_3)_3 \cdot 9H_2O$, $Ni(NO_3)_2 \cdot 6H_2O$, Na_2HPO_4 (99.0%), NaH_2PO_4 (99.0%) and ethylenediamine (99%) were obtained from Alfa-Aesar (Ward Hill, MA). GO was prepared according to the well-documented Hummers method (Hummers et al., 1958; Zhang et al., 2010). Deionized (DI) water produced by a Milli-Q Millipore system (18.2 MΩ cm, Millipore Corp., USA) was used for preparation of all the solutions. All chemicals and solvents were obtained from the commercial sources and used directly without any further purification.

2.2. Functionalization of CdSe/ZnS QDs with aptamer or complementary DNA (cDNA)

The water-soluble CdSe/ZnS QDs with the fluorescence emission at 569 nm were synthesized according to our previous reports (Li et al., 2011c, 2011d). The ligand-exchange was carried out to replace the hydrophobic trioctylphosphine oxide (TOPO) with hydrophilic mercaptopropionic acid (MPA). The aptamer or cDNA was then conjugated to the CdSe/ZnS QD by the well-established carbodiimide chemistry (Fig. S1) (Wang et al., 2011b; Yang et al., 2009). The carboxyl group-modified CdSe/ZnS QDs were mixed with 25 mM NHS and 100 mM EDC, and then incubated for 1 h to activate the carboxyl group. Subsequently, 10 μM aptamer or cDNA was added, and incubated for 24 h. The free excessive aptamer or cDNA was removed by centrifugation and washing with 10 mM PBS solution. The resulting aptamer or cDNA–QD conjugates were re-dispersed into 10 mM PBS solution and stored at 4 °C for further use.

2.3. Covalent functionalization of GO sheet with ssDNA

The carboxyl groups on the GO sheet were activated by adding 25 mM NHS and 100 mM EDC to the GO solution in a PBS solution (10 mM Na_2HPO_4/NaH_2PO_4, 0.3 M NaCl and pH = 7.0), and kept for 2 h. Subsequently, 4 μM ssDNA was added to 1 mL of 1 g/L GO solution with activated carboxyl groups, and incubated overnight. The ssDNA–GO conjugates were purified by filtration and centrifugation. Then, the ssDNA–GO conjugates were washed with a PBS buffer solution at least 5 times to remove free ssDNA. Finally, the ssDNA–GO conjugates were dispersed into a PBS solution with a final concentration of 2 g/L for further use.

2.4. GO–dsDNA–CdSe/ZnS QDs

To couple the QDs to GO through dsDNA, 200 μg/mL cDNA–GO solution was dropwise added to the cDNA–QD conjugates with a concentration of 300 nM in 10 mM PBS, and the fluorescence was monitored. After the resulting solution was incubated for 2 h, the fluorescence was then measured. All the sensing assays used in the work contained 10 mM Na_2HPO_4/NaH_2PO_4 and 0.3 M NaCl at a fixed pH = 7.0 if no further annotation. Here ethylenediamine was used as the chelating reagent to exclude the interference of other metal ions (Freeman et al., 2009; Li et al., 2011c).

2.5. Characterization and instrumentation

The morphology of GO was observed under the tapping mode with an atomic force microscopy (AFM) (Nanoscope V scanning probe microscope, Bruker, USA). Prior to AFM measurement, a drop of GO aqueous solution was deposited on a freshly cleaved mica surface and dried at room temperature. The aptamer–QD complex was observed with a JEM 2100 high-resolution transmission electron microscope (HRTEM, JEOL, Japan) at an operation voltage of 200 kV. The TEM sample was prepared with the supernatant solution after the solution containing GO/aptamer–QD ensemble was centrifuged at a speed of ~3000 rpm. Ultraviolet–visible absorption spectra were recorded with a Shimadzu UV-2550 spectrometer (Shimadzu Co., Kyoto, Japan). Fluorescence (FL) emission spectra were collected under the excitation of 400 nm with a HITACHI F-7000 fluorescence spectrophotometer (Hitachi High-Tech, Tokyo, Japan). Fourier transform infrared (FT-IR) spectra were acquired from the KBr pellet containing the sample under transmission mode with a Nicolet 6700 spectrometer (Thermo Scientific, Waltham, MA). Raman spectrum measurement was carried out with a Renishaw Invia Raman spectrometer (Renishaw PLC, Gloucestershire, UK) at the excitation laser of 532 nm with a 20× objective lens.

3. Results and discussion

3.1. Microstructure of nanoparticles

Fig. 1(a) and (b) show the AFM image of the as-prepared GO and the representative height profile, respectively. The height profile reveals that the GO sheets were 1.2 nm thick, which confirmed the monolayer structure of GO sheets (Li et al., 2012b; Loh et al., 2010). After the GO sheets were added into an aqueous solution containing the aptamer–QD complex, the aptamer–QD complex was bound onto the GO sheet to form the GO/aptamer–QD ensemble, which was confirmed by the TEM observation (Fig. 1(d)). More detailed information on the CdSe/ZnS QDs and GO can be found in Fig. S2.

3.2. Operating principle of sensor

The present fluorescent sensor is constructed based on the principle of energy transfer. When the QDs conjugated with the ssDNA aptamer are suspended in an aqueous solution in the absence of the GO sheets, the aptamer–QD complex exhibits

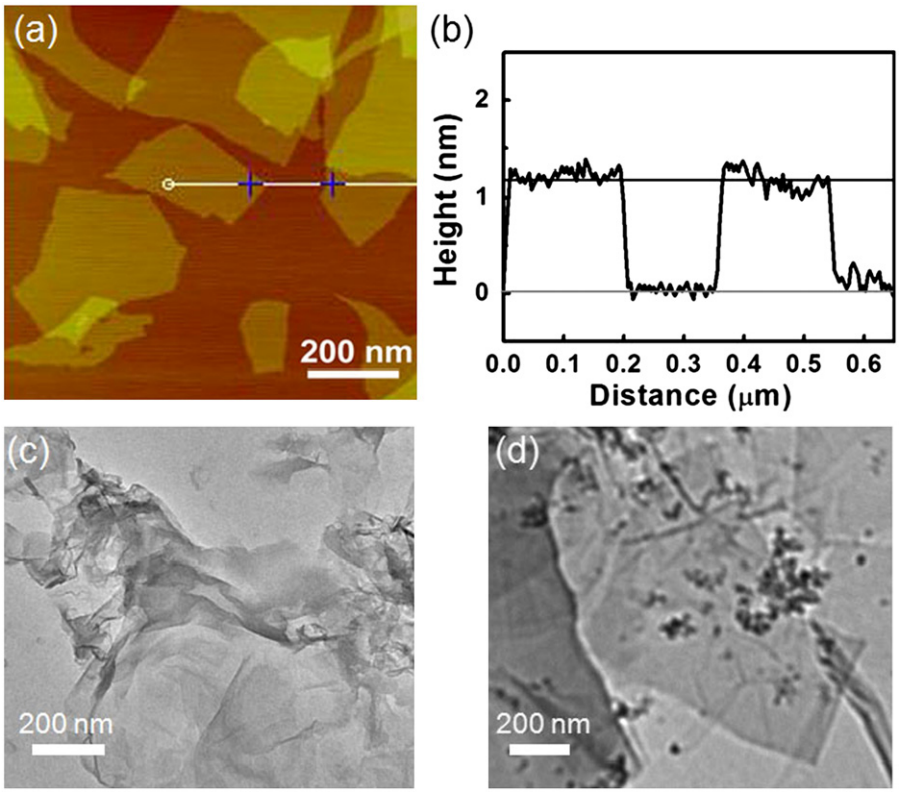

Fig. 1. AFM image (a) and height profile (b) of graphene oxide (GO) deposited on the mica substrate; TEM images of GO (c) and the GO/aptamer–QD complex (d).

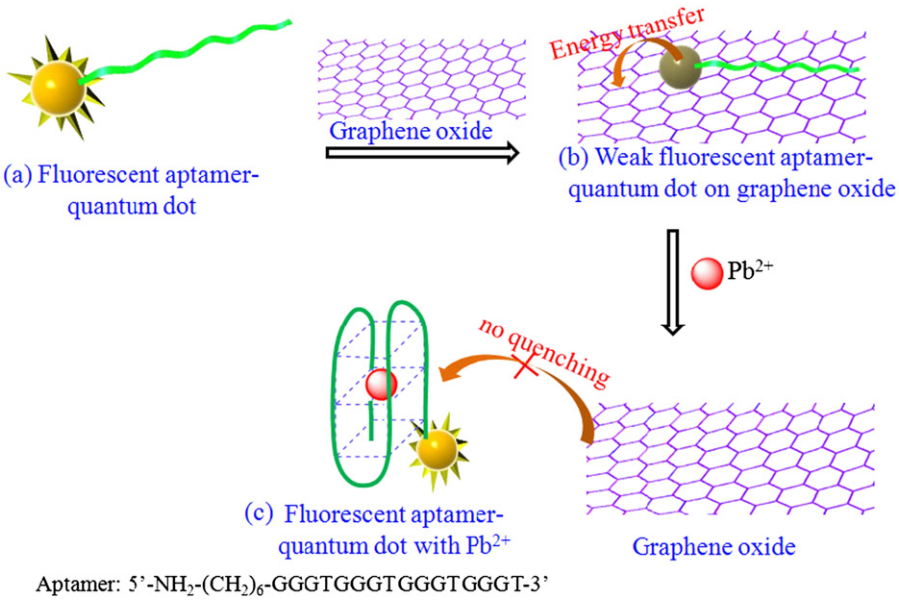

Fig. 2. Illustration of the operating principle of the "turn-on" fluorescent sensor for Pb^{2+} detection.

strong fluorescence emission at 567 nm (Fig. 2(a)). When the aptamer–QD complex is mixed with the GO sheets, the aptamer–QD complex particles are brought into the close proximity with the surface of the GO sheet due to the π–π stacking interactions between the aromatic nucleobases of aptamer and the sp^2-bonded carbon atoms of GO (Guo and Dong, 2011; Patil et al., 2009; Wang et al., 2011a), which enables the energy transfer from the QDs to the GO sheet (Fig. 2(b)). As a result, the fluorescence emission of the QDs is quenched. The GO/aptamer–QD ensemble acts as the sensor platform for Pb^{2+} detection.

The GO/aptamer–QD ensemble is stable in the aqueous solution in the absence of Pb^{2+}. When the Pb^{2+} ions are present, the Pb^{2+} ions interact with the aptamer. Consequently, the aptamer undergoes a conformational change (Fig. 2(c)), leading to the formation of a G-quadruplex/Pb^{2+} complex. The π–π stacking interaction between the G-quadruplex/Pb^{2+} complex and GO is

weakened because the aromatic nucleobases are shielded within the negatively charged phosphate backbone in the complex (He et al., 2010; Chang et al., 2010). As a result, the QDs are detached from the GO sheet. Thus, the free-standing aptamer–QD complex emits the fluorescence under the excitation in the presence of Pb^{2+}. In short, the presence of Pb^{2+} ions "turns on" the fluorescence emission of the QDs by disabling the energy transfer between the QDs and the GO sheet. Generally, this kind of "turn-on" sensing strategy has better resistance to the background interference over a "turn-off" method (Li et al., 2010a, 2012b).

To examine the formation process of the GO/aptamer–QD ensemble, various concentrations of GO were added to the PBS solution containing 300 nM the aptamer–QD complex. Consequently, the fluorescence emission of the aptamer–QD complex decreased with an increase in the GO concentration (Fig. S3). Almost all fluorescence emission of QDs was quenched after 200 μg/mL GO was added (Fig. S3(b)). The complete quenching was due to several reasons: (i) when the GO concentration exceeded 200 μg/mL, all the QD–ssDNA complex particles were immobilized on the GO surface due to the strong π–π interaction between the GO and the ssDNA; (ii) since the ssDNA laid down on the GO surface, the QDs were in intimate contact with the GO surface, which maximized the quenching efficiency; and (iii) the GO had super quenching capability. Thus, a fixed GO concentration (200 μg/mL) was used for the next experiments.

Generally the pH value has a significant effect on the performance of GO–aptamer biosensor (Huang et al., 2011). For example, the pH value affects the affinity of the analyte to the aptamer. In this work, the pH value was fixed with the PBS buffer solution. The pH=7.0 was an optimized value, which has been demonstrated in the previous work (Li et al., 2010a, 2011a). In addition, 0.3 M NaCl was chosen as the suitable ionic strength. DNA hybridization becomes difficult at a low ionic strength (that is, a low level of NaCl) (Li et al., 2012a). The binding of analyte to the aptamer could become weak at a too high ionic strength due to the shielding effect of Na^+ ions (Hianik et al., 2007).

The kinetics of fluorescence recovery was examined in the presence of 100 nM Pb^{2+} by monitoring the fluorescence intensity as a function of time (Fig. 3(a)). The fluorescence intensity initially increased rapidly as the reaction time progressed, and then became slow. Finally, the maximum fluorescence intensity reached after 25 min. This was the assay time for Pb^{2+} detection, which was in agreement with the previous study (Chang et al., 2010). It should be noted that the fluorescence cannot be completely recovered to the initial status of aptamer–QDs in the absence of GO in the assay. Only about 90% of fluorescence of the aptamer–QDs was recovered.

3.3. Detection of Pb^{2+}

The sensor employed in the present work was the GO/aptamer–QD ensemble assay. Fig. 3(b) shows the fluorescence spectra of the GO/aptamer–QD ensemble assay upon addition of various concentrations of Pb^{2+}. The GO/aptamer–QD ensemble assay exhibited a very weak fluorescence emission in the absence of Pb^{2+}. After the Pb^{2+} ions were added, the fluorescence of the aptamer–QD was recovered (Fig. 3(b)). Fig. 3(c) shows the calibration curve of the sensor. The linear response range of the sensor was determined to be 0.1–10 nM. In the linear response range, the calibration curve can be described by the equation $[(F-F_0)F_0]=1.6302\cdot[Pb^{2+}]+0.5475$ with the coefficient of determination (R^2) of 0.9943. F and F_0 represented the fluorescence intensity of the QDs at 567 nm in the presence and absence of Pb^{2+}, respectively. A limit of detection (LOD), which was defined as 3 times standard deviation/slope by the International Union of Pure and Applied Chemistry (IUPAC) standard, was determined to be 90 pM (0.019 ppb). The high sensitivity of the sensor may be attributed to the super quenching capability of GO, the significant difference in the affinity of aptamer toward

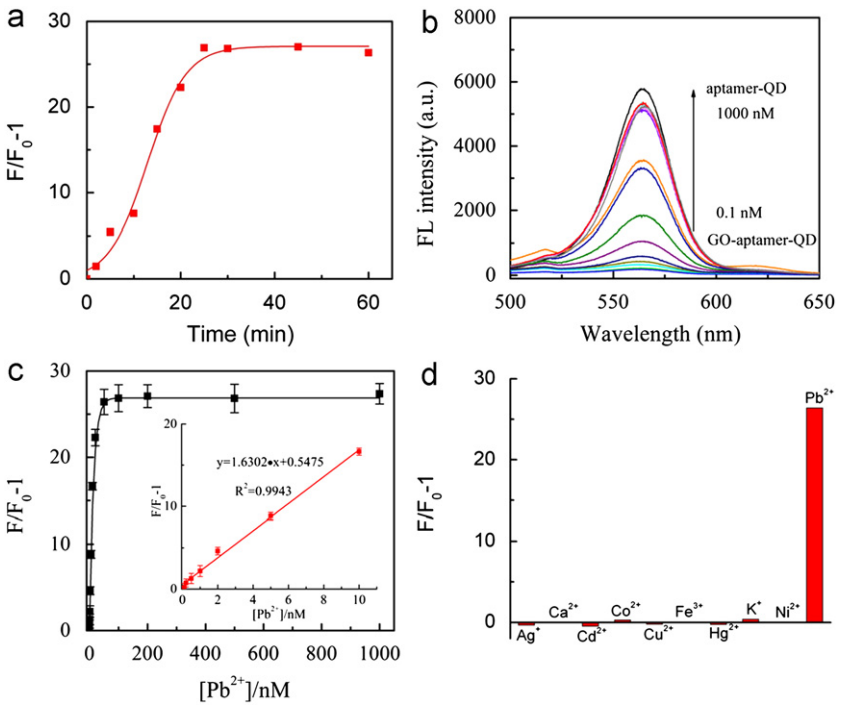

Fig. 3. (a) Time-dependent relative fluorescence intensity of the GO/aptamer–QD ensemble in the presence of 100 nM Pb^{2+}. (b) Fluorescence spectra of the GO/aptamer–QD ensemble assay upon addition of Pb^{2+} from 0 to 1000 nM (300 nM aptamer–QDs, 200 μg/mL GO, 10 mM PBS, 0.3 M NaCl, 0.1 mM ethylenediamine, and pH=7.0); (c) Relative fluorescence intensity of the GO/aptamer–QD ensemble assay as a function of Pb^{2+} concentration. Inset: The linear range of the sensing assay. (d) Selectivity of the GO/aptamer–QD ensemble assay toward Pb^{2+} over other metal ions of 500 nM ($[Pb^{2+}]=50$ nM, [other metal ions]=500 nM). F_0 and F are the fluorescence intensity at 567 nm in the presence and absence of Pb^{2+} or other metal ions, respectively.

Pb^{2+} and GO, as well as the low background signal of the "turn-on" fluorescent sensor. The performance of our sensor was compared with the previously reported Pb^{2+} sensors including fluorescent, colorimetric, and electrochemical devices, as listed in Table S1 (Jiang et al., 2010; Li et al., 2010a, 2010b; Wang et al., 2012; Zhao et al., 2011b). It can be seen that our sensor showed 1–3 orders of magnitude lower LOD than most of the sensors reported previously.

Selectivity is another performance parameter for a practical sensor. To test the selectivity, the fluorescence response of the GO/aptamer–QD ensemble assay was tested against other metal ions including Ag^{+}, Ca^{2+}, Cd^{2+}, Co^{2+}, Cu^{2+}, Fe^{3+}, Hg^{2+}, Ni^{2+} and K^{+}. It can be seen from Fig.3(d) that no evident change in the fluorescence of the GO/aptamer–QD ensemble assay was observed when any other metal ion was present in the assay except for Pb^{2+}. The presence of Ag^{+}, Cd^{2+}, Cu^{2+} or Hg^{2+} caused a slight fluorescence quenching ($F/F_0-1<-0.24$) while Co^{2+} or K^{+} led to a little increase in the fluorescence intensity ($F/F_0-1<0.4$). Ca^{2+}, Fe^{3+} or Ni^{2+} induced no observable change in the fluorescence intensity. This result showed that the GO/aptamer–QD ensemble assay exhibited excellent selectivity toward Pb^{2+} over a wide range of metal ions, which may be attributed to high specificity of the aptamer toward Pb^{2+} through the formation of a G-quadruplex structure (Li et al., 2010a, 2011a).

3.4. Measurement of Pb^{2+} in river water

To test the applicability of the developed sensor in the real aquatic environment, the Pb^{2+} concentration in the aqueous solution containing real-world river water was measured with the sensor (Fig. 4). The river water was collected from the Monongahela River near our campus. Prior to testing, the collected river water was filtered by a filter paper (Millipore, Isopore membrane). 1 mL of the river water sample was mixed with 1 mL of the PBS solution containing the aptamer–QD complex, which resulted in a solution with 300 nM aptamer–QDs. Prior to measure the Pb^{2+} ions, the resulting solution was adjusted to 200 μg/mL GO, 0.3 M NaCl and 0.1 mM ethylenediame in the PBS buffer solution. It was found that the Pb^{2+} content in the river water was too low to be detected. Hence extra Pb^{2+} ions were added into the assay. The fluorescence intensity increased with an increase in the Pb^{2+} concentration. In this case, the LOD of the sensing assay was observed to be 260 pM (0.053 ppb), which was slightly higher than that in the pure PBS solution. This result indicated that the present sensor can be applied to detection of Pb^{2+} in river water.

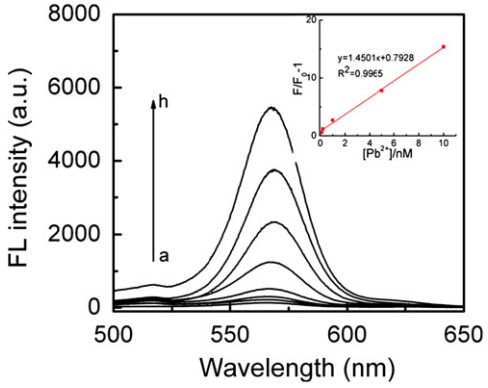

Fig. 4. The fluorescent response of the GO/aptamer–QD ensemble upon the addition of Pb^{2+} in the solution containing river water (300 nM aptamer–QD, 200 μg/mL GO, 0.3 M NaCl, 0.1 mM ethylenediamine and pH=7.0). The inset is the linear response range of the assay.

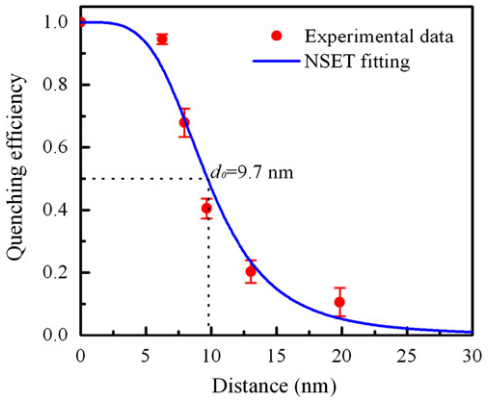

Fig. 5. Quenching efficiency of fluorescence as a function of GO-to-QD distance in the GO–dsDNA–CdSe/ZnS QD system. The experimental data were fitted using the equation $E=1/[1+(d/d_0)^4]$, and d_0 is the separation distance at the quenching efficiency of 50%.

3.5. Fluorescence quenching mechanism by GO

The fluorescence of QDs could be quenched by GO *via* three possible mechanisms: (i) charge transfer, (ii) FRET and (iii) nano-metal surface energy transfer (NSET) mechanism. The difference among three mechanisms has been described in our previous papers (Li et al., 2011c, 2011d). Briefly, for the charge transfer mechanism, the quenching efficiency is exponentially decayed with an increase in the distance between the fluorophore and the quencher. In the FRET process, the energy transfer efficiency depends on the $1/d^6$, where d is the separation distance between the energy donor and the acceptor. In the NSET process, the energy transfer efficiency has a correlation of $1/d^4$ with the separation distance. To clarify which mechanism was responsible for the fluorescence quenching of QDs by the GO sheet, the energy transfer was measured through controlling the separation distance with different dsDNA lengths (10 base pairs (bp), 15 bp, 20 bp, 30 bp and 50 bp). The DNA sequences used were listed in Table S2 in Supporting Information. Fig. 5 shows the distance-dependent fluorescence quenching efficiency. It can be seen that the quenching efficiency decreased with an increase in the separation distance. The experimental data was fit into the equation $E=1/(1+(d/d_0)^4)$, which was consistent with the trend predicted by the NSET theory. The characteristic distance (d_0) that corresponded to the separation distance at the quenching efficiency of 50% was calculated to be 9.7 nm. This result suggested that the NSET mechanism played a dominant role in fluorescence quenching of QDs by GO, which was in agreement with the previous report that the energy transfer from QDs to the two dimensional carbon film follows the NSET energy transfer mechanism (Jander et al., 2011).

4. Conclusions

In summary, in the GO/aptamer–QD system, the energy transfer from the QD to GO followed the NSET mechanism. The energy transfer efficiency depended on the $1/d^4$ separation distance. A fluorescent Pb^{2+} sensor was designed based on the NSET mechanism. The Pb^{2+}-specific aptamer conjugated with the QDs was adsorbed onto the GO surface through the π–π interaction, which brought the QDs into the close proximity with the GO sheet. As a result, energy transfer occurred from the QDs to the GO sheet, consequently "turned off" the fluorescence emission of the QDs. This resulted in the formation of a GO/aptamer–QD ensemble assay whose fluorescence emission can be "turned-on"

by the presence of trace Pb^{2+} ions. Such a sensing assay exhibited a limit of detection as low as 90 pM and an excellent selectivity toward Pb^{2+}. In addition, the sensor can be applied to the river water sample for Pb^{2+} detection. It is believed that the sensing platform/mechanism can be adapted for detection of other analytes such as heavy metal ions, small molecules and biomolecules.

Acknowledgment

This work was financially supported by a NSF grant (CBET-0754405). The resource and facilities used were partially supported by NSF (EPS 1003907) and a Research Challenge Grant from the State of West Virginia (EPS08-01), the West Virginia University Research Corporation and the West Virginia EPSCoR Office. N.W. is also grateful to the partial support of the George D. Hott Memorial and John Mathew Gay Brown Family Foundation. The use of the WVU Shared Research Facilities was acknowledged.

Appendix A. Supporting information

Supplementary data associated with this article can be found in the online version at http://dx.doi.org/10.1016/j.bios.2012.11.039.

References

Balapanuru, J., Yang, J.X., Xiao, S., Bao, Q.L., Jahan, M., Polavarapu, L., Wei, J., Xu, Q.H., Loh, K.P., 2010. Angewandte Chemie International Edition 49, 6549–6553.
Chang, H., Tang, L., Wang, Y., Jiang, J., Li, J., 2010. Analytical Chemistry 82, 2341–2346.
Chen, J.-L., Yan, X.-P., Meng, K., Wang, S.-F., 2011. Analytical Chemistry 83, 8787–8793.
Crivat, G., Silva, S.M.D., Reyes, D.R., Locascio, L.E., Gaitan, M., Rosenzweig, N., Rosenzweig, Z., 2010. Journal of the American Chemical Society 132, 1460–1461.
Darbha, G.K., Ray, A., Ray, P.C., 2007. ACS Nano 1, 208–214.
De, M., Chou, S.S., Dravid, V.P., 2011. Journal of the American Chemical Society 133, 17524–17527.
Dong, H., Gao, W., Yan, F., Ji, H., Ju, H., 2010. Analytical Chemistry 82, 5511–5517.
Dulkeith, E., Ringler, M., Klar, T.A., Feldmann, J., 2005. Nano Letters 5, 585–589.
Freeman, R., Finder, T., Willner, I., 2009. Angewandte Chemie International Edition 121, 7958–7961.
Gaponik, N., Hickey, S.G., Dorfs, D., Rogach, A.L., Eychmüller, A., 2010. Small 6, 1364–1378.
Goyer, R.A., 1993. Environmental Health Perspectives 100, 177–187.
Guo, S., Dong, S., 2011. Journal of Materials Chemistry 21, 18503–18516.
He, S., Song, B., Li, D., Zhu, C., Qi, W., Wen, Y., Wang, L., Song, S., Fang, H., Fan, C., 2010. Advanced Functional Materials 20, 453–459.
Hianik, T., Ostatná, V., Sonlajtnerova, M., Grman, I., 2007. Bioelectrochemistry 70, 127–133.
Huang, P.-J., Kempaiah, R., Liu, J., 2011. Journal of Materials Chemistry 21, 8991–8993.
Hummers, W.S., Offeman, R.E., 1958. Journal of the American Chemical Society 80, 1339.
Jennings, T.L., Singh, M.P., Strouse, G.F., 2006. Journal of the American Chemical Society 128, 5462–5467.
Jander, S., Kornowski, A., Weller, H., 2011. Nano Letters 11, 5179–5183.
Jiang, Z., Fan, Y., Liang, A., Wen, G., Liu, Q., Li, T., 2010. Plasmonics 5, 375–381.
Kong, L., Wang, J., Zheng, G., Liu, J., 2011. Chemical Communications 47, 10389–10391.
Lee, J., Kim, Y.-K., Min, D.-H., 2011. Analytical Chemistry 83, 8906–8912.
Li, F., Feng, Y., Zhao, C., Li, P., Tang, B., 2012a. Chemical Communications 48, 127–129.
Li, F., Feng, Y., Zhao, C., Tang, B., 2011a. Chemical Communications 47, 11909–11911.
Li, J., Lu, C.H., Yao, Q.H., Zhang, X.L., Liu, J.J., Yang, H.H., Chen, G.N., 2011b. Biosensors and Bioelectronics 26, 3894–3899.
Li, J., Wu, Y., Song, F., Wei, G., Cheng, Y., Zhu, C., 2012b. Journal of Materials Chemistry 22, 478–482.
Li, M., Wang, Q., Shi, X., Hornak, L.A., Wu, N., 2011c. Analytical Chemistry 83, 7061–7065.
Li, M., Cushing, S.K., Wang, Q., Shi, X., Hornak, L.A., Hong, Z., Wu, N., 2011d. The Journal of Physical Chemistry Letters 2, 2125–2129.
Li, M., Li, R., Li, C.M., Wu, N.Q., 2011e. Frontiers in Bioscience S3, 1308–1331.
Li, M., Zhou, X., Ding, W., Guo, S., Wu, N.Q., 2013. Biosensors and Bioelectronics 41, 889–893.
Li, M., Cushing, S.K., Zhou, X., Guo, S., Wu, N.Q., 2012d. Journal of Materials Chemistry 22, 23374–23379.
Li, T., Dong, S., Wang, E., 2010a. Journal of the American Chemical Society 132, 13156–13157.
Li, T., Wang, E., Dong, S., 2010b. Analytical Chemistry 82, 1515–1520.
Ling, J., Huang, C.Z., 2010. Analytical Methods 2, 1439–1447.
Liu, J., Lu, Y., 2002. Journal of the American Chemical Society 124, 15208–15216.
Lu, C.-H., Yang, H.-H., Zhu, C.-L., Chen, X., Chen, G.-N., 2009. Angewandte Chemie International Edition 48, 4785–4787.
Loh, K.P., Bao, Q., Eda, G., Chhowalla, M., 2010. Nature Chemistry 2, 1015–1024.
Medintz, I.L., Clapp, A.R., Brunel, F.M., Tiefenbrunn, T., Tetsuouyeda, H., Chang, E.L., Deschamps, J.R., Dawson, P.E., Mattoussi, H., 2006. Nature Materials 5, 581–589.
Patil, A.J., Vickery, J.L., Scott, T.B., Mann, S., 2009. Advanced Materials 21, 3159–3164.
Peng, C., Hu, W., Zhou, Y., Fan, C., Huang, Q., 2010. Small 6, 1686–1692.
Quach, A.D., Crivat, G., Tarr, M.A., Rosenzweig, Z., 2011. Journal of the American Chemical Society 133, 2028–2030.
Shi, Y., Huang, W.T., Luo, H.Q., Li, N.B., 2011. Chemical Communications 47, 4676–4678.
Stankovich, S., Piner, R.D., Chen, X., Wu, N.Q., Nguyen, S.T., Ruoff, R.S., 2006. Journal of Materials Chemistry 16, 155–158.
Swathi, R.S., Sebastian, K.L., 2008. Journal of Chemical Physics 129, 054703.
Swathi, R.S., Sebastian, K.L., 2009. Journal of Chemical Physics 130, 086101.
Tan, G.L., Hömmerich, U., Temple, D., Wu, N.Q., Zheng, J.G., Loutts, G., 2003. Scripta Materialia 48, 1469–1474.
Wang, D., Zhao, H., Wu, N.Q., El Khakani, A., Ma, D., 2010a. The Journal of Physical Chemistry Letters 1, 1030–1035.
Wang, H., Xu, W., Zhang, H., Li, D., Yang, Z., Xie, X., Li, T., Liu, X., 2011a. Small 7, 1987–1992.
Wang, H.B., Zhang, Q., Chu, X., Chen, T.T., Ge, J., Yu, R.Q., 2011b. Angewandte Chemie International Edition 50, 7065–7069.
Wang, Y., Li, Z., Hu, D., Lin, C.-T., Li, J., Lin, Y., 2010b. Journal of the American Chemical Society 132, 9274–9276.
Wang, Y., Li, Z., Wang, J., Li, J., Lin, Y., 2011. Trends in Biotechnology 29, 205–212.
Wang, Z., Qin, Y., Wang, C., Sun, L., Lu, X., Lu, X., 2012. Applied Surface Science 258, 2017–2021.
Wei, W., Xu, C., Ren, J., Xu, B., Qu, X., 2012. Chemical Communications 48, 1284–1286.
Xiang, C., Li, M., Zhi, M., Manivannan, A., Wu, N.Q., 2013. Journal of Power Sources 226, 65–70.
Yang, M., Kabulski, J.L., Wollenberg, L., Tracy, T.S., Subramanian, M., Lederman, D., Gannett, P.M., Wu, N.Q., 2009. Drug Metabolism and Disposition 37, 892–899.
Yun, C.S., Javier, A., Jennings, T., Fisher, M., Hira, S., Peterson, S., Hopkins, B., Reich, N.O., Strouse, G.F., 2005. Journal of the American Chemical Society 127, 3115–3119.
Zhang, C., Yuan, Y., Zhang, S., Wang, Y., Liu, Z., 2011a. Angewandte Chemie International Edition 50, 6851–6854 37.
Zhang, J., Yang, H., Shen, G., Cheng, P., Zhang, J., Guo, S., 2010. Chemical Communications 46, 1112–1114.
Zhang, M., Yin, B.C., Tan, W.H., Ye, B.C., 2011b. Biosensors and Bioelectronics 26, 3260–3265.
Zhang, M., Yin, B.C., Wang, X.F., Ye, B.C., 2011c. Chemical Communications 47, 2399–2401.
Zhao, H., Chaker, M., Wu, N.Q., Ma, D., 2011a. Journal of Materials Chemistry 21, 8898–8904.
Zhao, X.-H., Kong, R.-M., Zhang, X.-B., Meng, H.-M., Liu, W.-N., Tan, W., Shen, G.-L., Yu, R.-Q., 2011b. Analytical Chemistry 83, 5062–5066.